



Article

Multimethod Approach to the Study of Recent Volcanic Ashes from Tengger Volcanic Complex, Eastern Java, Indonesia

Nono Agus Santoso ^{1,*}, Satria Bijaksana ¹ , Kazuto Kodama ² , Djoko Santoso ¹ and Darharta Dahrin ¹

¹ Faculty of Mining and Petroleum Engineering, Institut Teknologi Bandung, Bandung 40132, Indonesia; satria@fi.itb.ac.id (S.B.); dsantoso@gf.itb.ac.id (D.S.); dahrin@gf.itb.ac.id (D.D.)

² Research Center for Knowledge Science in Cultural Heritage, Doshisha University, Kyoto 610-0394, Japan; kdma@kochi-u.ac.jp

* Correspondence: nonoagussantoso2@gmail.com; Tel.: +62-856-4675-2221

Academic Editors: Marco Viccaro and Jesús Martínez Frías

Received: 17 April 2017; Accepted: 25 July 2017; Published: 26 July 2017

Abstract: Volcanic ash is a volcanic product with a wide distribution that can be used as a geological marker. In volcanic regions such as Indonesia, the identification of the sources of volcanic ash and tuff layers from different volcanoes or eruptive events is a challenging task. In this study, samples of volcanic ash from the 2010 eruption of Bromo—a relatively young and active tuff cone volcano within the Sandsea caldera in the Tengger volcanic complex in East Java, Indonesia—along with two older tuff layers from the same caldera (Widodaren tuff: 1.8 kyr and Segarawedi tuff: 33 kyr) were subjected to magnetic measurements, geochemical analyses, and petrographic analyses. The aim is to attempt to use magnetic characters as a fingerprint for volcanic ash and tuff layers. The results show that the samples had variations in grain size and magnetic domain as indicated by the hysteresis parameters. These magnetic characters correlated with the results of geochemical and petrographic analyses, suggesting that magnetic properties may potentially be used as fingerprints to identify volcanic ashes and tuff layers.

Keywords: 2010 Bromo ash; volcanic ash; magnetic characteristics; geochemistry; Tengger

1. Introduction

According to the PVMBG (Pusat Vulkanologi dan Mitigasi Bencana Geologi—Indonesian Center for Volcanology and Mitigation of Geological Hazards), the Bromo volcano (latitude 7.942° S; longitude 112.95° E) is one of the most active volcanoes amongst Indonesia's 129 active volcanoes [1]. Since 1995, Bromo has erupted every five years with a duration of approximately one year [1]. Bromo is located in the Sandsea caldera of the Tengger Volcanic Complex in East Java, which houses other older and extinct volcanoes, namely Widodaren, Segarawedi Lor, Segarawedi, and Kursi-Watangan (Figure 1). Next to Bromo is the young and yet inactive Batok volcano. Tuff layers from Widodaren and Segarawedi have been dated to 1.8 kyr and 33 kyr, respectively [2]. Based on the stages of evolution for the Tengger Volcanic Complex, the Sandsea caldera is actually the youngest (late Pleistocene to early Holocene) caldera [3]; the two older ones are the Agrowulan and Ngadisari calderas [2]. The Bromo activity is considered to have been initiated sometime prior to ~1800 years BP.

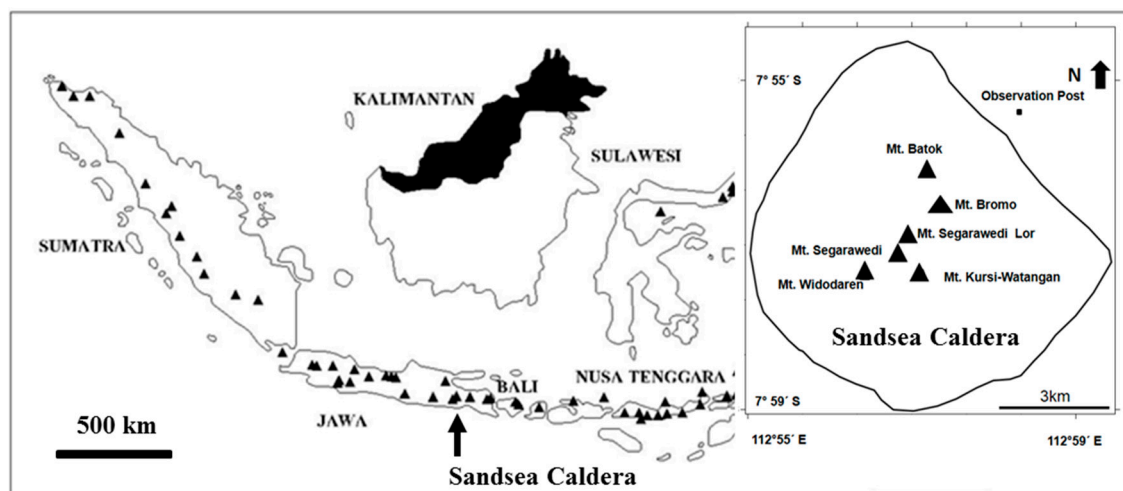


Figure 1. Distribution of volcanoes in Indonesia and the location of the Sandsea caldera.

Due to its activity and impact on the local populations, Bromo has been the subject of many different studies. For instance, Gottschämer and Surono [4] determined the locations of the tremor sources and shock signals based on seismic signals recorded during a phase of high eruptive activity in 1995. Abidin et al. [5] used GPS surveys to detect the deformation of Bromo. Later, Kumalasari and Srigutomo [6] used an inversion scheme to estimate the magma chamber location and volume change contributing to the surface deformation. Apart from physical studies, there have also been chemical studies on Bromo. Bani et al. [7] studied sulfur dioxide emissions from Bromo and Papandayan, the other active volcano in West Java. Later, using in situ Multi-Gas analysis and remote spectroscopic measurements, Aiuppa et al. [8] measured the composition and fluxes of volcanic gases released by Bromo. The social aspect of Bromo and its inhabitants has also been studied, where Bachri et al. [9] investigated the reasons why people chose to live near Bromo despite the exposure to volcanic hazards and found that the interaction between humans and the volcanic environment at Bromo was multifaceted and complex.

Despite its abundant volume, volcanic ash (such as that from the 2010 Bromo eruption) has never been studied, especially with regard to rock magnetic aspects. Only a few studies exist that combine rock magnetic methods with the more common methods of petrographic and geochemical analyses studies are available in the literature. Cicchino et al. [10] measured the geochemistry, as well as the magnetic remanence and AMS (anisotropy of magnetic susceptibility), of two islands in the Aeolian Islands to improve the stratigraphic correlation between the deposits cropping out on these two islands. Oda et al. [11] carried out rock magnetic and geochemical analyses on volcanic ash particles extracted from tephra-bearing ice samples collected from the Nansen Ice Field south of the Sør Rondane Mountains (Antarctica) and found that the magnetic mineral in the volcanic particles was titanomagnetite with an ulvöspinel content of 0.2–0.35 (in 0 to 1 scale). Oda et al. [11] also compared the geochemistry of the volcanic ash with that of three tephra layers from three different locations in Antarctica and found that these samples had a high geochemical similarity. The source of the tephra layers was suspected to be South Sandwich Island, located 2800 km from the Sør Rondane Mountains. Additionally, working with volcanic ash from several volcanoes, Pawse et al. [12] found that hysteresis measurements and electron spin resonance (ESR) spectroscopy may be used to identify and correlate distal volcanic ash.

The identification of volcanic ash could be very important as geological markers in volcanic regions such as Indonesia. Volcanic ash has usually been used for stratigraphic correlation and age measurements [13–15]. In Indonesia, volcanic ash and tuff layers from different volcanoes or different eruptive events of the same volcano may be deposited at a particular location as overlapping layers [16,17]. This study aimed to obtain an overview of the magnetic characteristics of the Bromo

volcanic ash in a maiden attempt to use magnetic characters as fingerprints for volcanic ash. Magnetic characterization focused on the volcanic ash from the 2010 eruption due to its extended eruption period and its enormous volume. As a comparison, tuff layers from earlier eruptions from the same caldera were also measured. To complement the magnetic methods, petrographic and X-ray Fluorescence (XRF) was also conducted on the same set of samples.

2. Materials and Methods

Samples of 2010 Bromo volcanic ash were obtained from the Indonesian Geological Survey Bromo Volcano Observational Post whose personnel collected ash during the 2010–2011 Bromo eruption. The tuff layers of Segarawedi and Widodaren were collected from an outcrop (Figure 2) in the vicinity of the aforementioned observational post. The observation post is located in the rim of the Sandsea caldera (Figure 1) at an elevation of 2275 m a.s.l. It administratively belongs to the Ngadisari Village, Sukapura District, Probolinggo Regency, East Java Province (latitude 7.942° S, longitude 112.950° E).

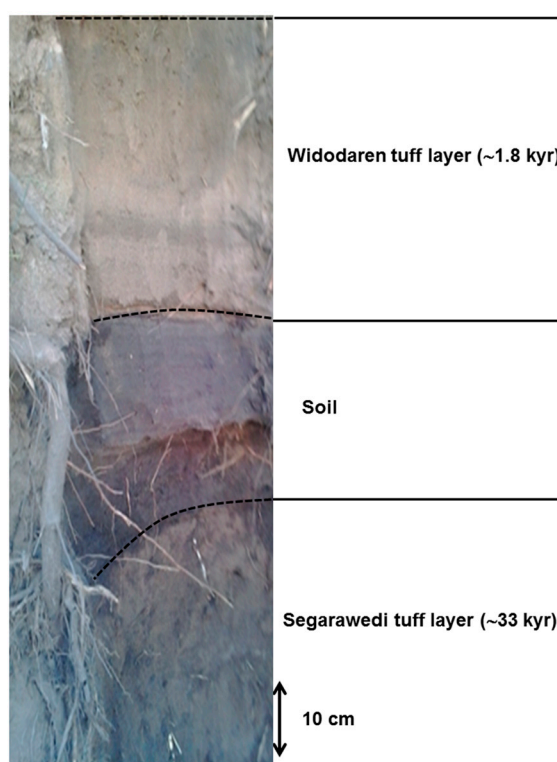


Figure 2. Outcrop of tuff layers.

The dry powder samples were brought to the Institut Teknologi Bandung (Bandung) where they were prepared for petrographic, geochemical, and magnetic susceptibility measurements. For simplicity, in this paper, the 2010 Bromo ash, Widodaren dan Segarawedi tuffs will be referred to as separate events (i.e., 2010 Bromo event, Widodaren event and Segarawedi event). Each event was represented by a single sample for petrographic analysis and analyzed with a Ci-POL polarizing microscope (Nikon, Tokyo, Japan) in the Petrographic Laboratory, Institut Teknologi Bandung. Later, each event was represented by a single sample for geochemical analysis using XRF (ARLX OPTX-2050, Thermo Fisher Scientific, Reinach, Switzerland) with a maximum current of 10 mA, maximum voltage of 50 kV, and maximum power of 200 W at the Nanotech Laboratory in Serpong. Mass-specific magnetic susceptibility was measured using a Bartington MS2B magnetic susceptibility system (Bartington Instrument Ltd., Witney, UK) with a dual-frequency sensor (470 Hz and 4700 Hz) at the Laboratory of Rock Magnetism at the Institut Teknologi Bandung. Mass-specific magnetic susceptibility

at low frequency was termed χ_{LF} , while that at high frequency was termed χ_{HF} . Parameter frequency-dependent magnetic susceptibility χ_{FD} (%) was calculated as $100\% \times (\chi_{LF} - \chi_{HF})/\chi_{LF}$. The total number of samples for magnetic susceptibility measurements were 15, where each event was represented by five samples. The samples were then subjected to ARM (anhysteretic remanent magnetization) analyses, where ARM was induced inside a Molspin AF (alternating field) demagnetizer (Molspin Ltd., Witney, UK) in a steady field of 0.05 mT imposed on a peak alternating magnetic field of 70 mT. Next, the ARM intensity was measured using a Minispin magnetometer (Molspin Ltd.). The ARM was then demagnetized using the AF demagnetizer in steps of 5 mT until it reached 70 mT, where the remaining ARM was less than 10% of its original value. After each demagnetizing step, the ARM intensity was remeasured using a Minispin magnetometer.

Three samples for each event were then analyzed for trace elements using atomic absorption spectroscopy (AAS; Agilent FS 280, Agilent Technologies, Santa Clara, CA, USA) for Cr, and inductively coupled plasma optical emission spectrometry (ICP OES Agilent Series 700) for Y, La, Zr, Ce, and V. These measurements were carried out in a laboratory at the Coal and Geothermal Mineral Resources Center at the Ministry of Energy and Mineral Resources in Bandung. Later, the samples were transported to the Rock Magnetic Laboratory in the Center of Advanced Marine Core Research, Kochi University, Japan where they were prepared for further magnetic analysis that included isothermal remanent magnetization (IRM), thermomagnetic, and magnetic hysteresis parameters. The measurement of magnetic hysteresis parameters and IRM were conducted using a vibrating sample magnetometer (VSM) (MicroMag 3900, Princeton Measurement Co., Princeton, NJ, USA) on dry powder samples. Five samples from each event (2010 Bromo ash, Widodaren tuff and Segarawedi tuff) were measured for the hysteresis parameters, while three samples from each event were measured for IRM. Magnetic hysteresis parameters were produced with a maximum applied field of 1 T and applied field increments of 2 mT. IRM saturation curves were produced by applying successive magnetic fields of 0 mT to a maximum field of 1 T with field increments of 2 mT. Each event was represented by a single sample for thermomagnetic analyses using a Magnetic Balance (NMB-89, Natsuhara Giken, Osaka, Japan) equipped with a furnace and special power supply. Magnetization of the sample was measured during heating in a vacuum from 50 to 700 °C, then subsequently during cooling back to room temperature.

3. Results and Discussion

Table 1 shows the results of the XRF analyses for the 2010 Bromo ash, Widodaren tuff, and Segarawedi tuff. Data from the Merapi ash [18] and Toba tuff [19] were also listed for comparison. The Merapi ash came from the 2010 eruption [18], the same year as the Bromo ash. Although they belong to different volcanic systems, Bromo and Merapi are only approximately 280 km apart. Toba tuff was used only as a reference. Data from Table 1 were then plotted in Figure 3a,b. Figure 3a shows the plots of $\text{Na}_2\text{O} + \text{K}_2\text{O}$ versus SiO_2 (as proposed by Le Bas et al. [20]) for all samples, and shows that the 2010 Bromo ash, Widodaren tuff, Segarawedi tuff, and Merapi ash plotted close to each other and could be considered as basaltic trachy-andesite, while the Toba tuff was a rhyolite. As expected, when plotted in Miyashiro's plot [21] of FeO/MgO versus SiO_2 (see Figure 3b), the 2010 Bromo ash, Widodaren tuff, Segarawedi tuff, Merapi ash, and Toba tuff belonged to the tholeiitic magma series.

Table 2 lists the results of the trace element analyses. After plotting one trace element against another, it was found that the plots of Y versus Cr (as proposed by Rollinson [22]) were the best plots to distinguish between the volcanic ash in this study (Figure 4). As seen in Figure 4, samples from each event clustered together so that each event could be distinguished easily. The range of Y and Cr values for all samples fell within the volcanic-arc basalts [22]; and both Y and Cr were often used as fractionation indexes in volcanic-arc basalts [22].

Table 3 lists the results of the mass-specific magnetic measurements for the samples. Data from the Tiva Canyon tuff were used only for comparison [17]. Our results showed that the average χ_{LF} value of the 2010 Bromo ash was $464.98 \times 10^{-8} \text{ m}^3/\text{kg}$, which was higher than that of the Widodaren tuff

($354.64 \times 10^{-8} \text{ m}^3/\text{kg}$) and lower than that of the Segarawedi tuff ($530.26 \times 10^{-8} \text{ m}^3/\text{kg}$). The results were comparable with the Tiva Canyon tuff at 12 cm depth, which had a χ_{LF} of $500 \times 10^{-8} \text{ m}^3/\text{kg}$ [16]. Table 3 also shows that the average χ_{FD} (%) values for all samples varied only slightly around 3.5%, suggesting a small or negligible contribution of superparamagnetic (SP) grains.

Table 1. Chemical composition of the samples (in weight %) based on X-ray fluorescence (XRF) measurements.

| Oxides | Bromo | Widodaren | Segarawedi | Merapi Ash ¹ | Toba Tuff ² |
|--------------------------------|-------|-----------|------------|-------------------------|------------------------|
| SiO ₂ | 50.70 | 54.09 | 54.22 | 54.69 | 77.24 |
| TiO ₂ | 1.17 | 1.05 | 1.04 | 0.74 | 0.06 |
| Al ₂ O ₃ | 17.09 | 18.23 | 18.82 | 19.29 | 12.54 |
| FeO | 10.93 | 9.57 | 9.29 | 7.76 | 0.85 |
| MnO | 0.20 | 0.19 | 0.18 | 0.19 | 0.07 |
| MgO | 2.22 | 2.04 | 2.00 | 2.25 | 0.05 |
| CaO | 7.58 | 6.08 | 5.90 | 8.12 | 0.78 |
| Na ₂ O | 4.15 | 4.40 | 4.24 | 3.73 | 3.10 |
| K ₂ O | 3.20 | 3.27 | 2.97 | 2.16 | 5.20 |
| P ₂ O ₅ | 0.54 | 0.60 | 0.59 | 0.30 | - |
| SO ₃ | 1.44 | - | 0.21 | 0.03 | - |
| Total | 99.22 | 99.52 | 99.46 | 99.28 | 100.00 |

¹ Merapi ash [12]; ² Toba tuff [13].

Table 2. Results of trace elements analysis.

| Sample | Y (ppm) | Cr (ppm) | La (ppm) | Zr (ppm) | Ce (ppm) | V (ppm) |
|--------------|---------|----------|----------|----------|----------|---------|
| Bromo 1 | 18.12 | 18 | 13.84 | 130.14 | 40.66 | 40 |
| Bromo 2 | 18.71 | 20 | 14.94 | 133.60 | 46.14 | 40 |
| Bromo 3 | 18.33 | 19 | 13.78 | 129.97 | 42.42 | 40 |
| Widodaren 1 | 18.53 | 13 | 15.73 | 134.14 | 42.86 | 40 |
| Widodaren 2 | 19.21 | 13 | 15.09 | 141.28 | 45.92 | 40 |
| Widodaren 3 | 18.86 | 12 | 14.26 | 151.76 | 44.57 | 40 |
| Segarawedi 1 | 16.34 | 20 | 14.50 | 127.44 | 41.51 | 60 |
| Segarawedi 2 | 17.29 | 19 | 14.31 | 119.37 | 41.52 | 40 |
| Segarawedi 3 | 16.47 | 20 | 13.96 | 123.40 | 42.78 | 60 |

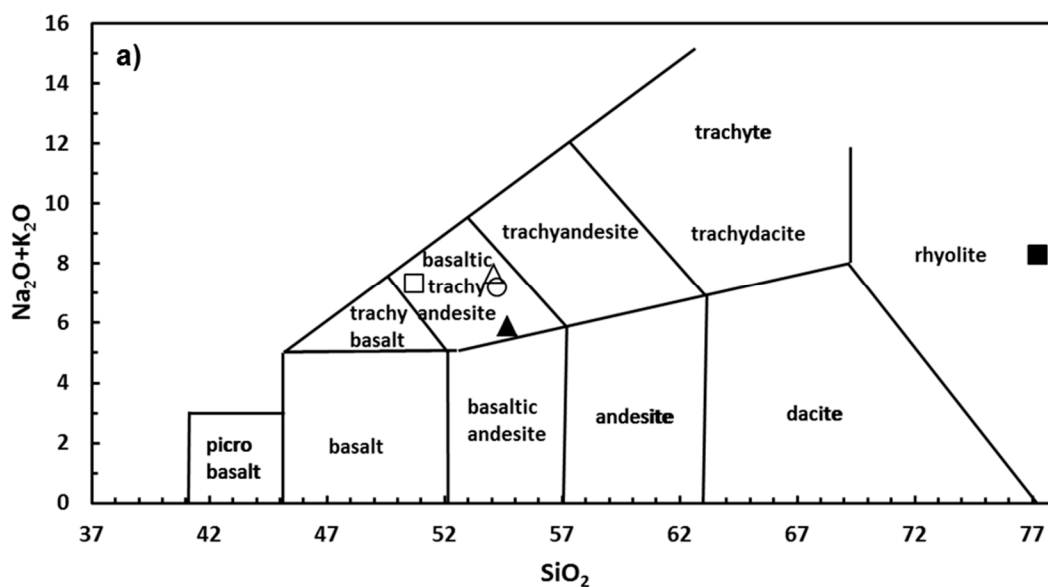


Figure 3. Cont.

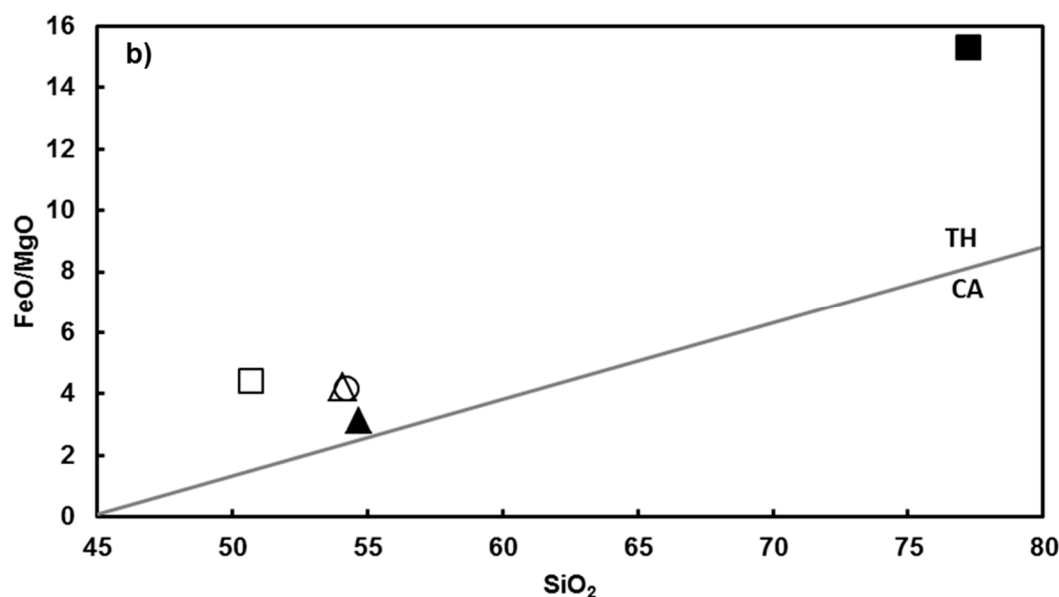


Figure 3. (a) SiO_2 versus $\text{Na}_2\text{O} + \text{K}_2\text{O}$ diagram [14]; and (b) FeO/MgO versus SiO_2 diagram [15] of the 2010 Bromo ash (hollow square), Widodaren tuff (hollow triangle), Segarawedi tuff (hollow circle), Merapi ash (filled triangle) and Toba tuff (filled square). TH: tholeiitic, CA: calc-alkaline.

Table 3. Results of magnetic susceptibility measurements.

| Sample | χ_{LF} ($\times 10^{-8} \text{ m}^3/\text{kg}$) | Average χ_{LF} ($\times 10^{-8} \text{ m}^3/\text{kg}$) | χ_{HF} ($\times 10^{-8} \text{ m}^3/\text{kg}$) | Average χ_{HF} ($\times 10^{-8} \text{ m}^3/\text{kg}$) | χ_{FD} (%) | Average χ_{FD} (%) |
|--------------|---|---|---|---|-----------------|-------------------------|
| Bromo 1 | 462.5 | 464.98 ± 2.54 | 444.6 | 448.54 ± 3.98 | 3.87 | 3.54 ± 0.57 |
| Bromo 2 | 465.5 | | 446.1 | | 4.17 | |
| Bromo 3 | 462.2 | | 447.7 | | 3.14 | |
| Bromo 4 | 467.8 | | 454.9 | | 2.76 | |
| Bromo 5 | 466.9 | | 449.4 | | 3.75 | |
| Widodaren 1 | 351.9 | 354.64 ± 10.79 | 338.5 | 341.04 ± 9.27 | 3.81 | 3.83 ± 0.34 |
| Widodaren 2 | 369.5 | | 353.5 | | 4.33 | |
| Widodaren 3 | 350.2 | | 336.8 | | 3.83 | |
| Widodaren 4 | 341.1 | | 329.6 | | 3.37 | |
| Widodaren 5 | 360.5 | | 346.8 | | 3.80 | |
| Segarawedi 1 | 530.1 | 530.26 ± 7.42 | 509.7 | 511.36 ± 6.45 | 3.85 | 3.56 ± 0.49 |
| Segarawedi 2 | 525.5 | | 505.1 | | 3.88 | |
| Segarawedi 3 | 521.5 | | 507.3 | | 2.72 | |
| Segarawedi 4 | 540.8 | | 521.6 | | 3.55 | |
| Segarawedi 5 | 533.4 | | 513.1 | | 3.81 | |

χ_{LF} : magnetic susceptibility at low frequency; χ_{HF} : magnetic susceptibility at high frequency; χ_{FD} : frequency-dependent magnetic susceptibility.

Figure 5a shows the IRM saturation curves for the 2010 Bromo ash samples along with those of the Widodaren and Segarawedi tuffs. All samples were saturated below the magnetizing field of 300 mT, implying that the predominant magnetic mineral in these samples was magnetite (Fe_3O_4). In addition, the second derivative curves of IRM over field [23] showed that each sample had a different coercivity spectrum (Figure 5b). This inferred that each sample had its own unique magnetic phase, which was also supported by the results of thermomagnetic analyses.

Figure 6a–c show the thermomagnetic curves for the 2010 Bromo ash samples, along with those of the Widodaren and Segarawedi tuffs. For all three samples, the heating curves showed double peaks that corresponded to the Hopkinson effect, i.e., a peak in magnetic susceptibility associated with Curie temperature [23]. The presence of magnetite with its distinctive Curie temperature (T_C) of $\sim 580^\circ\text{C}$ was obvious in the 2010 Bromo ash (Figure 6a) and Segarawedi tuff (Figure 6c), but was not so obvious in the Widodaren tuff (Figure 6b). Figure 6a–c also show that there was another magnetic

phase with a Curie temperature (T_c) of ~ 250 – 300 °C, indicating a titanomagnetite phase with a Ti substitution of 0.4–0.5 [24]. Such variations may explain the dissimilarity in IRM saturation curves for all samples (Figure 5a); moreover, the presence of two different magnetic phases was most likely due to the mechanisms that govern crystallization of iron-rich melt. Such mechanisms might include temperature variation, changes in chemistry prior to eruption, and increases in the redox conditions of the silicate melt [25]. The presence of these two different magnetic phases also reinforced the notion that new magma injection occurred during the Bromo eruption of 2010.

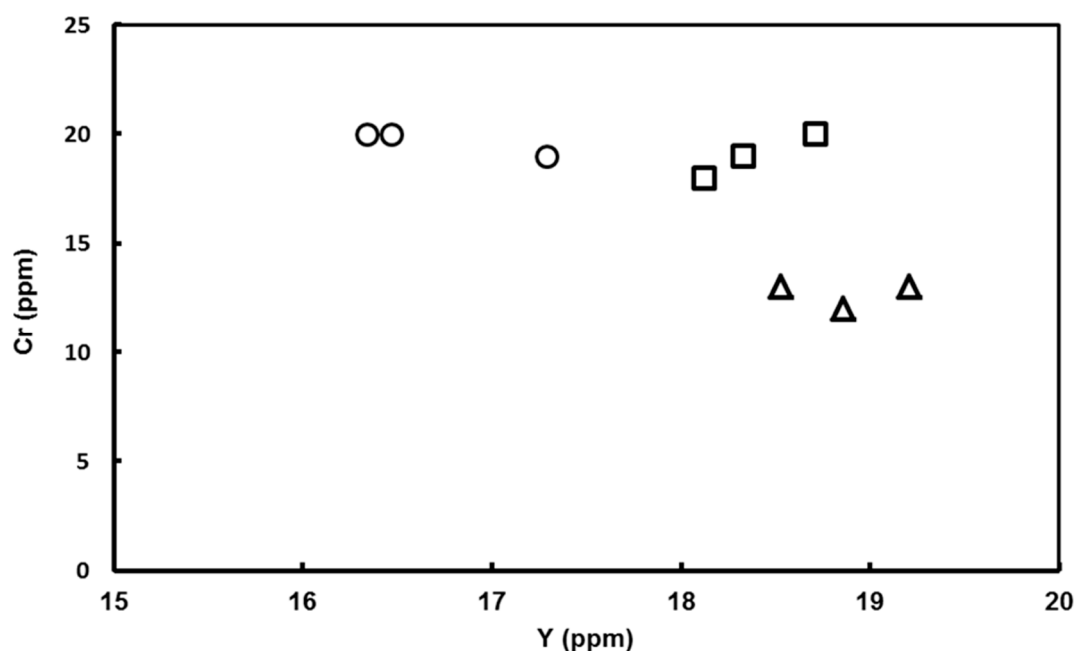


Figure 4. Y vs. Cr diagram of the 2010 Bromo ash (hollow square), Widodaren tuff (hollow triangle), and Segarawedi tuff (hollow circle).

Figure 7 shows the ARM demagnetization curves for the 2010 Bromo ash samples, along with those from the Widodaren and Segarawedi tuffs. By assuming that magnetite was the predominant magnetic mineral in these samples, the magnetic grain sizes of these samples could be estimated from the value of MDF (median destructive field) [26,27]. Figure 7 shows that the MDF of the 2010 Bromo ash and Segarawedi tuff were 15 mT and 25 mT corresponded to a grain size of 3–6 μm for the 2010 Bromo ash and 0.6–1 μm for Segarawedi tuff, respectively (as described in [26]), which represented the PSD (pseudo-single domain). Meanwhile, the Widodaren tuff sample showed a much lower MDF of 5 mT that corresponded to a grain size of >135 μm , which represented the MD (multi domain).

The petrographic analyses showed that the 2010 Bromo ash contained glass fragments (60%), crystal fragments (20%), and lithic or tuff fragments (20%). Meanwhile, the Widodaren tuff contained glass fragments (60%), crystal fragments (35%), and pores (5%). In contrast, the Segarawedi tuff contained mostly lithic fragments (65%), as well as lower quantities of glass (25%) and crystal (10%) fragments. Crystal fragments in all events consisted of plagioclase, pyroxene, and opaque minerals. The above finding suggests that the 2010 Bromo ash and Widodaren tuff experienced fast cooling processes during their deposition, while the Segarawedi tuff experienced a slow cooling process during its deposition. However, a fast cooling process does not necessarily produce multi domain magnetite. Ferk et al. [28] reported that, unlike single domain (SD) magnetite, PSD and MD magnetite was not affected by an increase or decrease of the cooling rate.

Table 4 shows the ratios of the magnetic hysteresis parameters. Data from Table 4 were plotted in Figure 8 (as suggested by Day et al. [29]) to identify the grouping of the samples based on their magnetic domains. Figure 8 shows that the samples from each event (2010 Bromo, Widodaren, and

Segarawedi) clustered together. The 2010 Bromo ash and Segarawedi samples were clustered in the PSD region, while the Widodaren samples were clustered in the MD region, thus supporting the results of the ARM analyses. However, despite all samples (2010 Bromo, Widodaren, and Segarawedi) being basaltic trachy-andesite, each event was still differentiable based on its hysteresis parameters. Care, however, should be taken when interpreting the Day's plot [29] on a mixture of SD and MD magnetite, or a mixture of magnetite and titanomagnetite [30,31]. These results show that magnetic hysteresis is the most promising and effective magnetic measurement for distinguishing volcanic ash.

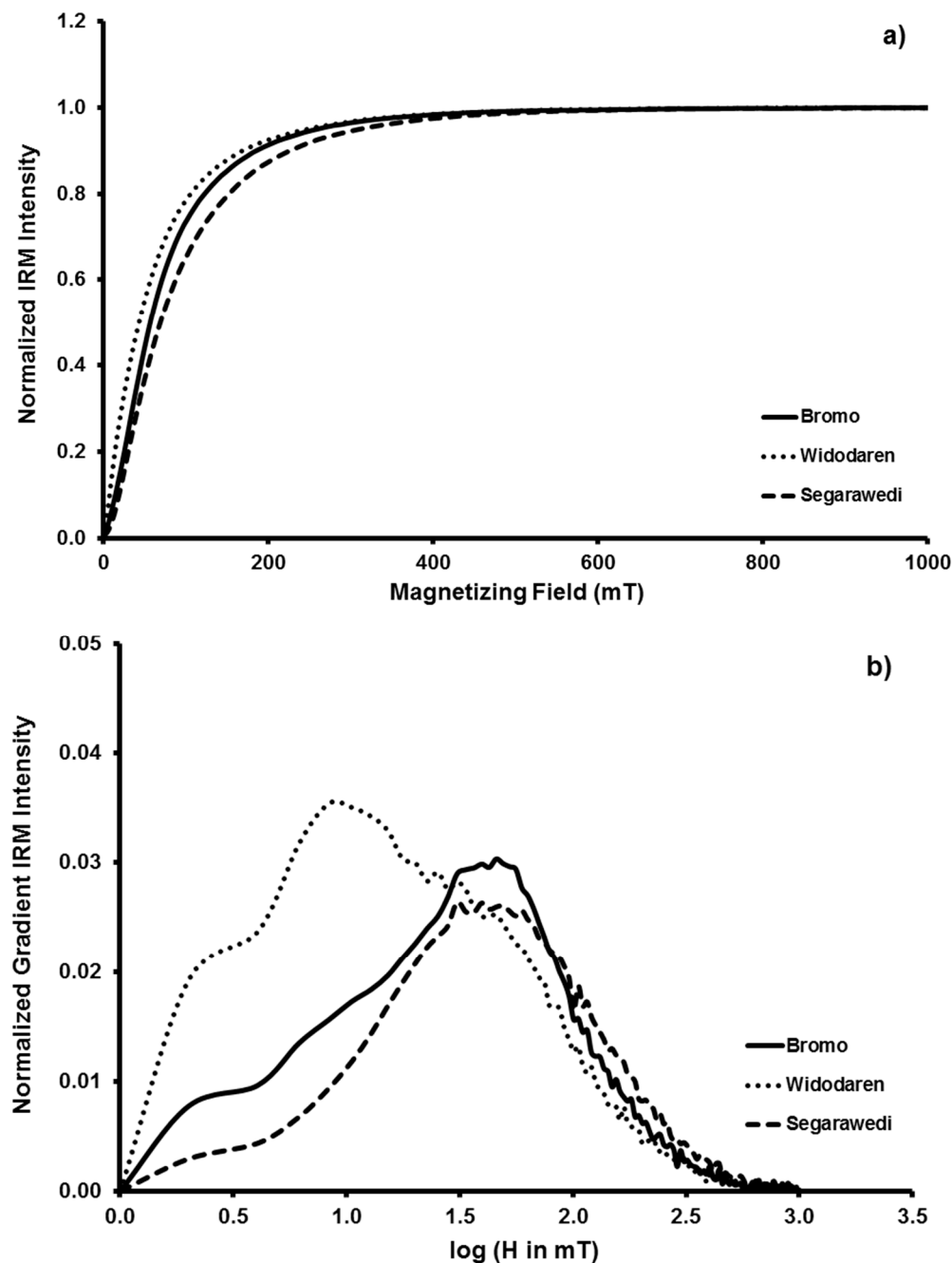


Figure 5. (a) The isothermal remanent magnetization (IRM) curves of the volcanic ash and tuff samples; and (b) the distribution of magnetic coercivity samples. H: magnetizing field.

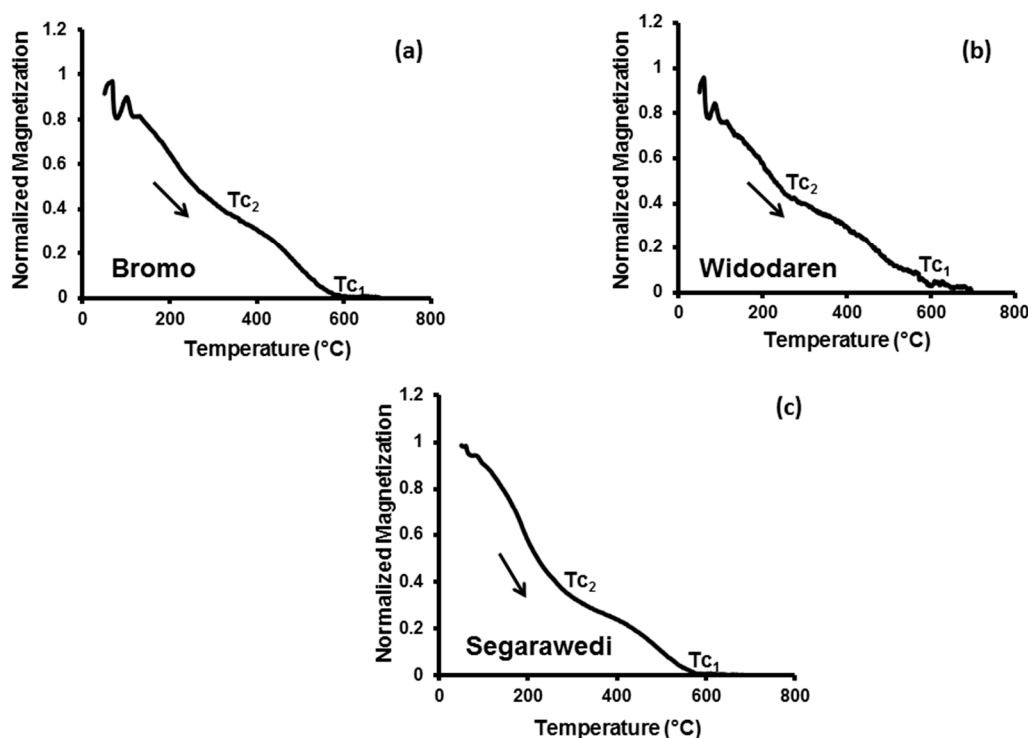


Figure 6. Thermomagnetic curves for (a) 2010 Bromo ash; (b) Widodaren tuff; and (c) Segarawedi tuff samples. T_{c1} : first Curie temperature; T_{c2} : second Curie temperature.

Table 4. Ratios of hysteresis parameters for samples.

| Name of Volcano/Event | Sample Code | M_r/M_s | B_{cr}/B_c |
|-----------------------|-------------|-----------|--------------|
| Bromo 1 | BM1 | 0.19 | 3.35 |
| Bromo 2 | BM2 | 0.19 | 3.26 |
| Bromo 3 | BM3 | 0.19 | 3.35 |
| Bromo 4 | BM4 | 0.21 | 2.89 |
| Bromo 5 | BM5 | 0.20 | 3.05 |
| Widodaren 1 | WD1 | 0.10 | 5.23 |
| Widodaren 2 | WD2 | 0.10 | 4.72 |
| Widodaren 3 | WD3 | 0.11 | 4.51 |
| Widodaren 4 | WD4 | 0.10 | 4.98 |
| Widodaren 5 | WD5 | 0.10 | 4.77 |
| Segarawedi 1 | SW1 | 0.26 | 2.46 |
| Segarawedi 2 | SW2 | 0.26 | 2.54 |
| Segarawedi 3 | SW3 | 0.25 | 2.55 |
| Segarawedi 4 | SW4 | 0.25 | 2.58 |
| Segarawedi 5 | SW5 | 0.26 | 2.51 |

M_r : remanence magnetization; M_s : saturation magnetization; B_{cr} : coercivity of remanence magnetic field; B_c : coercivity magnetic field.

The distinct magnetic characteristics of the 2010 Bromo ash, and Widodaren and Segarawedi tuffs shown in this study may serve as an initial step in using magnetic characteristics as fingerprints for volcanic ash and tuff layers. Earlier attempts by Xia et al. [14] to correlate the tephra layers using magnetic signatures in Iceland showed that the individual tephra did not have unique magnetic signatures, and that a correlation of the tephra layers could only be achieved through complex statistical techniques. This study showed that combined with trace element analyses, magnetic measurements (especially hysteresis measurement) could be used to potentially distinguish between the eruption

events of volcanic ashes and tuffs. This study even showed that the three samples (2010 Bromo ash, Widodaren tuff, and Segarawedi tuff) originated from the same caldera, and that a similar composition of major elements could have distinct magnetic signatures. Despite the positive results of this study, the use of magnetic parameters as correlation tools in volcanic ash layers should be tested further.

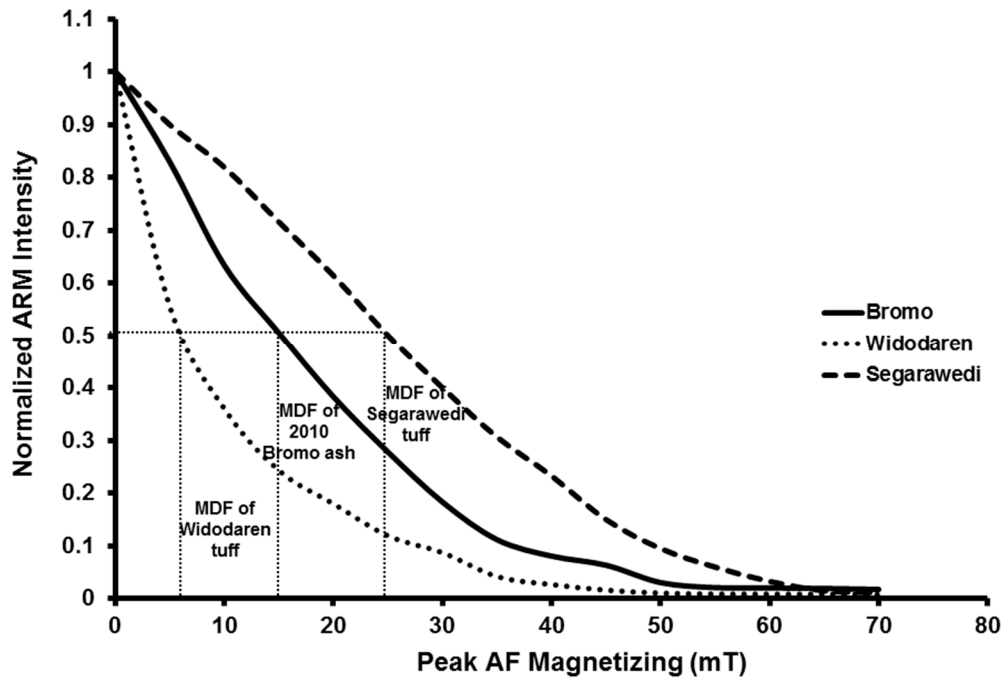


Figure 7. Anhyseretic remanent magnetization (ARM) decay curves of the volcanic ash and tuff samples. AF: alternating field; MDF: median destructive field.

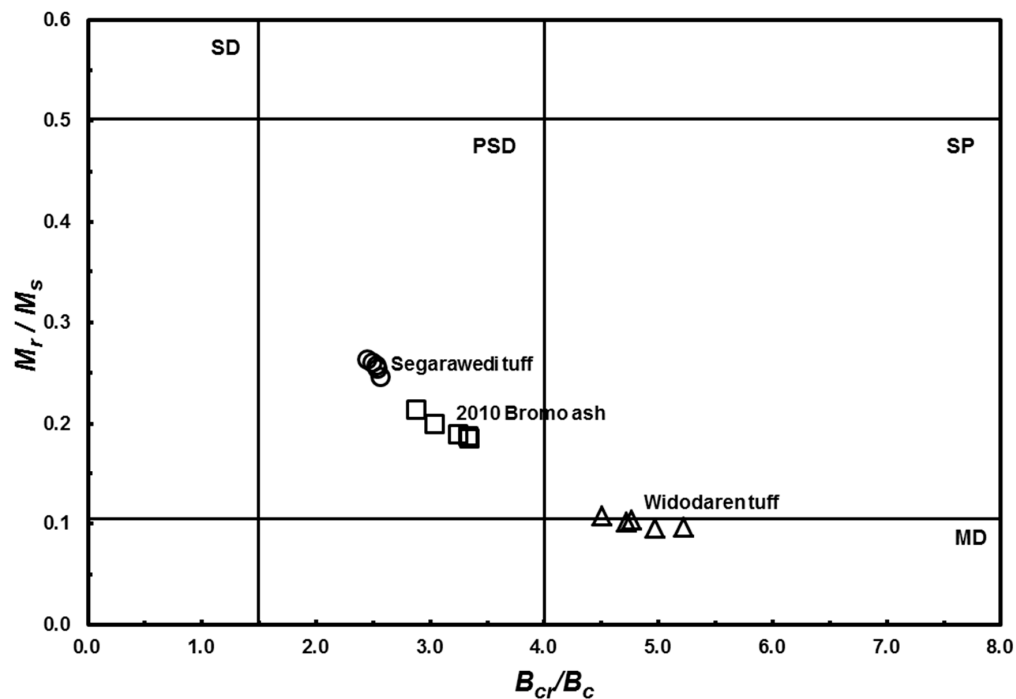


Figure 8. Plots of the hysteresis parameters on Day's plots [29] for the 2010 Bromo ash, Widodaren, and Segarawedi tuff samples. SD: single domain; PSD: pseudo single domain; SP: superparamagnetic.

4. Conclusions

The predominant magnetic mineral in the 2010 Bromo ash was found to be Ti-rich titanomagnetite with PSD magnetite. Compared with tuff layers from earlier events (Widodaren and Segarawedi), there were some dissimilarities in magnetic characteristics including grain size, magnetic domain, and hysteresis parameters. Dissimilarities in these events were also found in Y versus Cr plots and in petrographic analyses. Thus, the applications of these three methods (magnetic, geochemistry, and petrographic) might be used to identify volcanic ash and tuff layers. However, the use of magnetic methods alone should be carried out cautiously, especially if the volcanic ash or tuff layer has undergone physical and chemical changes such as diagenesis. Furthermore, hysteresis parameters and Day's plots have been shown to be effective discriminating tools for identifying volcanic ash and tuff layers.

Acknowledgments: This study is financially supported by the PMDSU Grant from the Ministry of Research, Technology, and Higher Education of the Republic of Indonesia to N.A.S., S.B., and D.D. We thank the Center of Advance Marine Core Research, Kochi University for the use of magnetic instruments. Our thanks also go to Myriam Kars for her assistance in using these instruments. We thank the three anonymous reviewers for their constructive comments.

Author Contributions: N.A.S., S.B., D.S., and D.D. conceived and designed the experiments; N.A.S., S.B., and D.S. collected the samples; N.A.S., S.B., and K.K. performed the experiments; and N.A.S., S.B., D.S., K.K., and D.D. analyzed the data and wrote the paper.

Conflicts of Interest: The authors declare no conflict of interest.

References

1. PVMBG. Data Dasar Gunungapi Indonesia. Available online: <http://www.vsi.esdm.go.id/index.php/gunungapi/data-dasar-gunungapi/532-g-bromo> (accessed on 21 August 2015).
2. Zaennudin, A. The Stratigraphy and Nature of the Stratocone of Mt. Cemara Lawang in the Bromo–Tengger Caldera, East Java, Indonesia. Master's Thesis, Victoria University of Wellington, Wellington, New Zealand, 1990.
3. Van Gerven, M.; Pichler, H. Some aspects of the volcanology and geochemistry of the Tengger Caldera, Java, Indonesia: Eruption of a K-rich tholeiitic series. *J. Southeast Asian Earth Sci.* **1995**, *11*, 125–133. [[CrossRef](#)]
4. Gottschämmer, E.; Surono, I. Locating tremor and shock sources recorded at Bromo Volcano. *J. Volcanol. Geotherm. Res.* **2000**, *101*, 199–209. [[CrossRef](#)]
5. Abidin, H.Z.; Andreas, H.; Gamal, M.; Hendrasto, M.; Suganda, O.K.; Purbawinata, M.A.; Meilano, I.; Kimata, F. The deformation of Bromo volcano (Indonesia) as detected by GPS surveys method. *J. Glob. Position. Syst.* **2005**, *3*, 16–24. [[CrossRef](#)]
6. Kumalasari, R.; Srigutomo, W. Location and pressures change prediction of Bromo volcano magma chamber using inversion scheme. *J. Phys. Conf. Ser.* **2016**, *739*. [[CrossRef](#)]
7. Bani, P.; Hendrasto, M.; Gunawan, H.; Primulyana, S. Sulfur dioxide emissions from Papandayan and Bromo, two Indonesian volcanoes. *Nat. Hazards Earth Syst. Sci.* **2013**, *13*, 2399–2407. [[CrossRef](#)]
8. Aiuppa, A.; Bani, P.; Moussallam, Y.; Di Napoli, R.; Allard, P.; Gunawan, H.; Hendrasto, M.; Tamburello, G. First determination of magma derived gas emissions from Bromo volcano, eastern Java (Indonesia). *J. Volcanol. Geotherm. Res.* **2015**, *304*, 206–213. [[CrossRef](#)]
9. Bachri, S.; Stötter, J.; Monreal, M.; Sartohadi, J. The calamity of eruptions, or an eruption of benefits? Mt. Bromo human–volcano system a case study of an open-risk perception. *Nat. Hazards Earth Syst. Sci.* **2015**, *15*, 277–290. [[CrossRef](#)]
10. Cicchino, A.M.P.; Zanella, E.; DeAstis, G.; Lanza, R.; Lucchi, F.; Tranne, C.A.; Airolidi, G.; Mana, S. Rock magnetism and compositional investigation of Brown Tuffs deposits at Lipari and Vulcan (Aeolian Islands—Italy). *J. Volcanol. Geotherm. Res.* **2011**, *208*, 23–38. [[CrossRef](#)]
11. Oda, H.; Miyagi, I.; Kawai, K.; Suganuma, Y.; Funaki, M.; Imae, N.; Mikouchi, T.; Matsuzaki, T.; Yamamoto, Y. Volcanic ash in bare ice south of Sør Rondane Mountains, Antarctica: Geochemistry, rock magnetism and nondestructive magnetic detection with SQUID gradiometer. *Earth Planet Space* **2016**, *68*, 39. [[CrossRef](#)]

12. Pawse, A.; Beske-Diehl, S.; Marshall, S.A. Use of magnetic hysteresis properties and electron spin resonance spectroscopy for the identification of volcanic ash: A preliminary study. *Geophys. J. Int.* **1998**, *132*, 712–720. [[CrossRef](#)]
13. Bigazzi, G.; Bonadonna, F.P.; Centamore, E.; Leone, G.; Mozzi, M.; Nisio, S.; Zanchetta, G. New radiometric dating of volcanic ash layers in Periadriatic foredeep basin system, Italy. *Palaeogeogr. Palaeoclimatol. Palaeoecol.* **2000**, *155*, 327–340. [[CrossRef](#)]
14. Xia, D.; Chun, X.; Bloemendal, J.; Chiverrell, R.C.; Chen, F. Use of magnetic signatures to correlate tephra layers in Holocene loessial soil properties from a small region, SE Iceland. *Environ. Geol.* **2007**, *51*, 1425–1437. [[CrossRef](#)]
15. Hong, H.; Fang, Q.; Wang, C.; Churchman, G.J.; Zhao, L.; Gong, N.; Yin, K. Clay mineralogy of altered tephra beds and facies correlation between the Permian-Triassic boundary stratigraphic sets, Guizhou, South China. *Appl. Clay Sci.* **2017**, *143*, 10–21. [[CrossRef](#)]
16. Tamuntuan, G.; Bijaksana, S.; King, J.; Russel, J.; Fauzi, U.; Maryunani, K.; Aufa, N.; Safiuddin, L.O. Variation of magnetic properties in sediments from Lake Towuti, Indonesia, and its paleoclimatic significance. *Palaeogeogr. Palaeoclimatol. Palaeoecol.* **2015**, *420*, 163–172. [[CrossRef](#)]
17. Till, J.L.; Jackson, M.J.; Rosenbaum, J.G.; Solheid, P. Magnetic properties in ash flow tufa with continuous grain size variation: A natural reference for magnetic particle granulometry. *Geochem. Geophys. Geosyst.* **2011**, *12*, 1–10. [[CrossRef](#)]
18. Damby, D.E.; Horwell, C.J.; Baxter, P.J.; Delmelle, P.; Donaldson, K.; Dunster, C.; Fubini, B.; Murphy, F.A.; Nattrass, C.; Sweeney, S.; et al. The respiratory health hazard of tephra from the 2010 Centennial eruption of Merapi with implication for occupational mining of deposits. *J. Volcanol. Geotherm. Res.* **2013**, *261*, 376–387. [[CrossRef](#)]
19. Lane, C.S.; Chorm, B.T.; Johnson, T.C. Ash from the Toba super eruption in Lake Malawi shows no volcanic winter in East Africa at 75 ka. *Proc. Natl. Acad. Sci. USA* **2013**, *110*, 8025–8029. [[CrossRef](#)] [[PubMed](#)]
20. Le Bas, M.J.; Le Maitre, R.W.; Streckeisen, A.; Zanettin, B. A chemical classification of volcanic rocks based on the total alkali-silica diagram. *J. Petrol.* **1986**, *27*, 745–750. [[CrossRef](#)]
21. Miyashiro, A. Volcanic rock series in island arcs and active continental margins. *Am. J. Sci.* **1974**, *274*, 321–355. [[CrossRef](#)]
22. Rollinson, H.R. *Using Geochemical Data: Evaluation, Presentation, Interpretation*, 1st ed.; Pearson Education Limited: London, UK, 1993; p. 188.
23. Tauxe, L. *Essentials of Paleomagnetism*, 4th ed.; University of California Press: Berkeley, CA, USA, 2010; pp. 8–2–8–8.
24. Ubangoh, R.U.; Pacca, I.G.; Nyobe, J.B.; Hell, J.; Ateba, B. Petro-magnetic characteristics of Cameroon Line volcanic rocks. *J. Volcanol. Geotherm. Res.* **2005**, *142*, 225–241. [[CrossRef](#)]
25. Velasco, F.; Tornos, F.; Hanchar, J.M. Immiscible iron- and silica-rich melts and magnetite geochemistry at the El Laco volcano (northern Chile): Evidence for a magmatic origin for the magnetite deposits. *Ore Geol. Rev.* **2016**, *79*, 346–366. [[CrossRef](#)]
26. Dunlop, D.J.; Özdemir, O. *Rock Magnetism Fundamental and Frontiers*, 1st ed.; Cambridge University Press: Cambridge, UK, 1997; pp. 306–307.
27. Maher, B.A. Magnetic properties of some synthetic sub-micron magnetites. *Geophys. J. Int.* **1988**, *94*, 83–96. [[CrossRef](#)]
28. Ferk, A.; Leonhardt, R.; Hess, K.-U.; Koch, S.; Egli, R.; Krása, D.; Dingwell, D.B. Influence of cooling rate on thermoremanence of magnetite grains: Identifying the role of different magnetic domain states. *J. Geophys. Res. Solid Earth* **2014**, *119*, 1599–1606. [[CrossRef](#)]
29. Day, R.; Fuller, M.D.; Schmidt, V.A. Hysteresis properties of titanomagnetites: Grain size and composition dependence. *Phys. Earth Planet. Inter.* **1977**, *13*, 260–266. [[CrossRef](#)]
30. Dunlop, D.J. Theory and application of the Day plot (M_{rs}/M_s versus H_{cr}/H_c): 1. Theoretical curves and tests using titanomagnetite data. *J. Geophys. Res.* **2002**, *107*, 2056. [[CrossRef](#)]
31. Dunlop, D.J. Theory and application of the Day plot (M_{rs}/M_s versus H_{cr}/H_c): 2. Application to data for rocks, sediments, and soils. *J. Geophys. Res.* **2002**, *107*, 2057. [[CrossRef](#)]

